Appl. Magn. Reson. 5, 43–61 (1993)

Applied Magnetic Resonance

© Springer-Verlag 1993
Printed in Austria

An Approximate Method of Sideband Intensity Calculation in Magic Angle Spinning NMR

B.Q. Sun and A. Pines

Materials and Chemical Sciences Division, Lawrence Berkeley Laboratory
and Chemistry Department, University of California, Berkeley, USA

Received February 26, 1993

Abstract. A theory of sideband intensity is derived by expanding into a Taylor series the free induction decay observed under magic angle spinning (MAS). According to this procedure, the free induction decay signal is completely represented by a basis of irreducible tensors from rank zero to rank infinity. After averaging over all orientations, only the zero-order irreducible tensors contribute to the sideband intensities. Symmetry properties of the sidebands can be seen clearly in this expansion, and an approximate formula up to ninth order is obtained by truncating the series. Sideband intensities can be calculated rapidly with this formula. The results agree satisfactorily with the exact sideband intensities obtained by numerical simulation if the ratio of the anisotropy to the spinning speed, $\omega_0\delta/\omega_r$, is smaller than 3. The relationship of the sideband intensities with the moments of a MAS spectrum shows that the proposed method is an alternative to moment analysis when the spinning speed is not very slow. Anisotropic information about the chemical shift anisotropy interaction therefore can be extracted efficiently from experimental spectra by this approximate method.

1. Introduction

Nuclear magnetic resonance is widely used for studying structure and dynamics of solid materials. In contrast to the sharp spectral lines obtained from liquids, however, NMR resonance frequencies of polycrystalline or amorphous solid samples are severely broadened owing to the absence of fast isotropic tumbling. Such motion, where present, acts to average anisotropic interactions such as chemical shift anisotropy (CSA), dipolar, and quadrupolar couplings to zero. Where the necessary internal averaging does not occur, macroscopic motion generally has to be applied to the spin system to improve spectral resolution. Magic angle spinning (MAS), in which the sample rotates around an axis inclined at the magic angle ($\vartheta_m = 54.74°$) with respect to the external magnetic field H_0 today is the most common method used for this purpose.

MAS was first proposed by Andrew *et al.*, and Lowe in the late 1950s to suppress homogeneous broadening due to the dipolar interaction [1–3]. Later, Schaefer and Stejskal showed that CSA also can be averaged to zero by MAS [4]. In the extreme where the spinning speed far exceeds the breadth of the anisotropy, MAS yields the isotropic shift at the expense of any information concerning the anisotropy. This condition must be met for homogeneous broadening, such as that caused by homonuclear dipolar interactions. However, for inhomogeneous broadening (for example, CSA and the first-order quadrupolar interaction) sidebands develop around the isotropic peak if the spinning speed is smaller than the anisotropy [5]. Maricq and Waugh [6] subsequently proposed that the free induction decay (FID) signal be expanded as a series of moments in order to extract the anisotropic information from the sidebands. Herzfeld and Berger [7] also developed a general method, involving Bessel functions, to calculate sideband intensities. The anisotropic information is recovered by numerical simulation of he individual sideband intensities.

In this paper we propose a new method to calculate approximate sideband intensities rapidly without using a large data base. The method involves expanding the FID signal in a basis of irreducible spatial tensors in such a way that, when averaged over all orientations, only zero-rank irreducible tensors (scalar operators) contribute to the sideband intensities. Symmetry properties of the sidebands can be seen clearly in this expansion, and an approximate formula up to ninth-rank irreducible tensors is obtained by truncating the series. The dependence of sideband intensities on anisotropic parameters (δ, η) can then be expressed explicitly. With least square fitting programs, the extraction of the principal values of the chemical shift anisotropy from the sideband intensities obtained from MAS spectra can be performed quickly and easily. Comparison of sideband intensities calculated by this approximate method with those determined by moment analysis shows that the new method offers an effective alternative when the spinning speed is not very slow. Finally, the technique is used to calculate the centerband intensity after applying a TOSS pulse sequence [8, 9].

2. Theory

We start with a rare spin nuclear system (such as ^{13}C) in which nuclear spins interact with the external static magnetic field H_0 via anisotropic chemical shielding. According to the notation and conventions given by Mehring [10], we can represent the spin Hamiltonian as

$$\mathscr{H} = \omega_0 I_z + \omega_0 \bar{\sigma} I_z + \gamma_N \sum_{m=-2}^{2} (-1)^m A_{2-m} T_{2m} , \qquad (1)$$

where γ_N is the nuclear gyromagnetic ratio of the spin species involved, $\bar{\sigma}$ is the isotropic chemical shielding, I_z is the spin operator, and A_{2-m} and T_{2m} are the components of the second-rank irreducible spatial and spin tensors respectively. In Eq.(1) the first term represents the Zeeman interaction, while the second term is the isotropic chemical shift and the third term is the chemical shift anisotropy (CSA). The principal values, ϱ_{2m}, of the CSA tensor are given by

$$\varrho_{20} = \sqrt{\frac{3}{2}}\delta\,, \qquad \varrho_{\pm 2} = \frac{1}{2}\eta\delta\,, \qquad \varrho_{\pm 1} = 0\,. \tag{2}$$

The $A_{2,m}$ in Eq.(1), which reflect the orientation dependence of the CSA Hamiltonian, can be expressed as

$$A_{2m} = \sum_{m'=-2}^{2} D^{(2)}_{m'm}(\Omega)\varrho_{2m'}\,, \tag{3}$$

$D^{(2)}_{m'm}(\Omega)$ are the components of the Wigner rotation matrices and $\Omega = \Omega(\alpha,\beta,\gamma)$ are Euler angles.

After the spin Hamiltonian given in Eq.(1) is transformed into the rotating frame by the unitary operator $\exp(-i\omega_0 I_z t)$, the time dependent terms in the total Hamiltonian may be neglected under the first-order perturbation approximation, and the total Hamiltonian becomes

$$\mathscr{H} = \omega_0 A_{20} T_{20}\,, \tag{4}$$

assuming that the isotropic chemical shift ($\omega_0\bar{\sigma}$) is zero in this particular case.

As the sample rotates around a fixed axis inclined at an angle ϑ with respect to H_0, the external magnetic field, as viewed in the rotor frame, moves on a cone with a half-angle ϑ (see Fig. 1). In other words, the external magnetic field traverses the spinning trajectory of the sample, and the local fields determined by the CSA tensor change periodically. The component of the second-rank irreducible spatial tensor, A_{20}, thus becomes time dependent. Expressed in terms of the Wigner rotation matrices, the spin Hamiltonian in the rotating frame is given by

$$\mathscr{H} = \gamma_N T_{20} \sum_{m=-2}^{2} D^{(2)}_{m,0}(\Omega_r) A_{2m}\,, \tag{5}$$

where $\Omega_r = \Omega_r(0,\vartheta,\omega_r t)$, ϑ is the angle between the rotor axis and H_0, and $\omega_r t$ is the azimuth of the x-axis of the rotor frame with respect to H_0. In

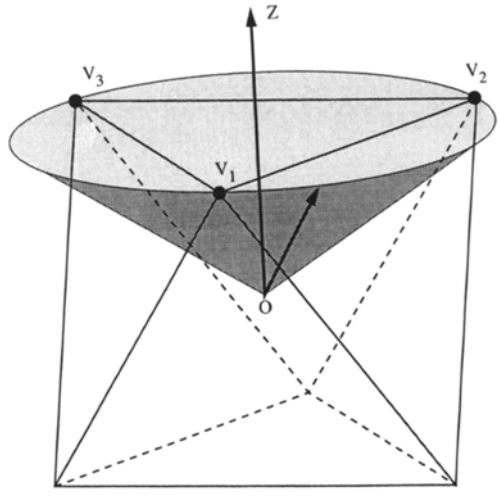

Fig. 1. The external magnetic field, viewed in the sample-fixed coordinate frame, travels on a magic angle cone with half-apex angle, $\vartheta_m = 54.74°$ under MAS. The magic angle cone crosses three vertices (V) of an octahedron.

Eq.(5), the time-independent part, corresponding to $m = 0$, disappears when $\vartheta = \vartheta_m$, the magic angle of the second-order Legendre polynomial. The remaining components in Eq.(5) are time dependent. Since the sample spinning is only applied on the spatial parts of the spin Hamiltonian, the spin Hamiltonian commutes with itself at all times. This means that the eigenvectors of the spin Hamiltonian remain unchanged, but the eigenvalues are modulated by a set of harmonics. Hence the resonance frequency becomes time dependent, and the FID signal for a spin $I = 1/2$ system can be written as

$$g(t) = \exp[-i\varphi(t)], \tag{6}$$

where

$$\varphi(t) = \sqrt{\frac{2}{3}} \frac{\omega_0}{-i\omega_r} \sum_{m=-2}^{2} \frac{d^{(2)}_{m,0}(\vartheta_m)}{m} A_{2,m} \varphi_m \tag{7}$$

and

$$\varphi_m = \exp(-imw_r t) - 1. \tag{8}$$

In general, Eq.(6) describes a phase-modulated signal with the associated Fourier spectrum showing a band structure. Each oriented single crystal contributes a particular sideband pattern, and what we see is the average over all orientations for a powder sample. Such an averaged sideband pattern is not related simply to the anisotropies and asymmetry parameters of

the CSA tensors, however. In order to extract these parameters from the experimental results obtained under MAS, Maricq and Waugh expanded Eq.(6) in a multiple moment series, and found that the second and third moments of the MAS NMR spectra are indeed related fairly simply to δ and η. In practical applications of the moment analysis method, the second and the third moments are first calculated from the sideband intensities and the spinning speeds of the sample obtained from the experimental MAS NMR spectra, and then, using the relationships between the moments and the principal values of the CSA tensors, the anisotropies and asymmetry parameters are obtained. Since the intensity of the N-th order sideband, in general, decays, as the sideband frequency increases, the contribution of small sideband intensity to the moments cannot be ignored. Therefore this method requires very accurate measurement of all sideband intensities, which is difficult to do. Moreover, the method fails when sidebands originating from different site in a spin system overlap. To overcome these problems, Herzfeld and Berger first expanded Eq.(6) using Bessel functions and subsequently converted it to a Fourier series. The N-th coefficient in the Fourier expansion then corresponds to the N-th sideband intensity. Nevertheless, the intensity of each sideband has a very complicated dependence on the anisotropic parameters, and the problem can be inverted only by time-consuming numerical simulations.

The dependence of the intensities on anisotropic parameters is complicated because the integrals over all orientations in Eq.(6) cannot be solved analytically. Taking a new approach, we will instead expand the FID signal in a Taylor series. By virtue of the properties of the products of two irreducible tensors, the FID signal is recast in a basis of irreducible tensors from rank zero the rank infinity. The rotational transformation properties of irreducible tensors yield analytical solutions for integrals up to any order.

The first step in this new method is to expand Eq.(6) into a Taylor series to obtain

$$g(t) = \sum_{\mathrm{k}} \frac{1}{k!} [\varphi(t)]^{\mathrm{k}} \,. \tag{9}$$

Substituting Eq.(7) into Eq.(9), we then have:

$$g(t) = \sum_{\mathrm{k}} \frac{1}{k!} \left(\sqrt{\frac{2}{3}} \frac{\omega_0 \delta}{\omega_{\mathrm{r}}} \right)^{\mathrm{k}} f_{\mathrm{k}}(t) \,, \tag{10}$$

where

$$f_{\mathrm{k}}(t) = \sum_{\mathrm{m}_1 \neq 0} \sum_{\mathrm{m}_2 \neq 0} \cdots \sum_{\mathrm{m}_{\mathrm{k}} \neq 0} B(m_1, m_2, \ldots, m_{\mathrm{k}}) \varphi_{\mathrm{m}_1} \varphi_{\mathrm{m}_2} \cdots \varphi_{\mathrm{m}_{\mathrm{k}}} A_{2,\mathrm{m}_1} A_{2,\mathrm{m}_2} \cdots A_{2,\mathrm{m}_{\mathrm{k}}} \tag{11}$$

and $$B(m_1, m_2, ..., m_k) = \frac{d^{(2)}_{m_1,0}(\vartheta_m)\, d^{(2)}_{m_2,0}(\vartheta_m) \ldots d^{(2)}_{m_k,0}(\vartheta_m)}{m_1 m_2 \ldots m_k \delta^k} . \quad (12)$$

Later, we will see that the function $f_k(t)$ depends only on the asymmetry parameter η.

In the next step, we introduce the product of two irreducible tensors given by [11]

$$A_{l_1,m_1} A_{l_2,m_2} = \sum_{l=|l_1-l_2|}^{l_1+l_2} C(l_1, l_2, l; m_1, m_2, m_1+m_2) A_{l,m_1+m_2} , \quad (13)$$

where $C(l_1,l_2,l;m_1,m_2,m_1+m_2)$ are the Clebsch-Gordan coefficients. Iterating using Eq.(13), we can represent the product of k second-rank irreducible tensors as

$$A_{2,m_1} A_{2,m_2} \ldots A_{2,m_k} = \sum_{l_1=0}^{4} \sum_{l_2=|l_1-2|}^{l_1+2} \ldots \sum_{l_{k-1}=|l_{k-2}-2|}^{l_{k-2}+2} C(2,2,l_1,m_1,m_2)$$

$$\times C(l_1,2,l_2,m_1+m_2,m_3) \ldots C(l_{k-2},2,l_{k-1}, \sum_{i=1}^{k-1} m_i, m_k) A_{l_{k-1}, \sum_{i=1}^{k} m_i} . \quad (14)$$

With the orientation dependence expressed in terms of the Wigner rotation matrices, the average of the l-th rank irreducible tensor over all orientations is

$$\overline{A_{l,m}} = \begin{cases} A_{0,0}(l_1, ..., l_{k-3}) & \text{if } l = 0 \text{ and } m = 0 \\ 0 & \text{otherwise} . \end{cases} \quad (15)$$

Hence only the scalar part in Eq.(11) remains after the powder average:

$$A_{0,0}(l_1, ..., l_{k-3}) = \sum_{n_1, \ldots n_{k-1} = -2}^{2} C(2,2,l_1,n_1,n_2) C(l_1,2,l_2,n_1+n_2) \ldots$$

$$C(2,2,0, \sum_{i=1}^{k-1} n_i, -\sum_{i=1}^{k-1} n_i) \varrho_{2,n_1} \varrho_{2,n_2} \ldots \varrho_{2,n_{k-1}} \varrho_{2,-\sum_{i=1}^{k-1} n_i} . \quad (16)$$

In this equation, the product of k components $\varrho_{2,n_i} (i=1...k)$ is of order δ^k, and will cancel with the δ^k in coefficient B of Eq.(11). Thus $f_k(t)$ is only a

function of the asymmetry factor η. From Eq.(2), the power of the asymmetry factor in $f_k(t)$ is determined by

$$n = \left[\frac{|n_1|}{2}\right] + \left[\frac{|n_2|}{2}\right] + \ldots + \left[\frac{|n_k|}{2}\right]. \tag{17}$$

The result of the square-brackets, representing the truncation of each individual term in Eq.(17), is an integer with the value zero or one. Since, from Eq.(3), ϱ_{n_i} are unequal to zero only if $n_i = 0, \pm 2$, and since, according to Eq.(15), the sum over all indices, $\Sigma_{i=1}^{k} n_i$, must be zero after the powder average, the number of indices with values of 2 must equal the number of indices with values of -2. Thus Eq.(17) can only result in an even integer. The power of η must be even and, consequently, the sideband intensities are not sensitive to the sign of the asymmetry factor. It follows, then, that sample rotation does not change the symmetry of the spin system, in agreement with the relationship between the static powder lineshapes and the asymmetry parameters η ($0 \leqq \eta \leqq 1$).

The symmetry of the coefficients B can be easily found after the powder average by use of the properties of reduced Wigner rotation matrices:

$$B(m_1, m_2, \ldots, m_k) = (-1)^k B(-m_1, -m_2, \ldots, -m_k). \tag{18}$$

In the final step, from Eqs.(14) and (15) we have $m_k = \Sigma_{i=1}^{k-1} m_i$. Inserting this condition into Eq.(11), we obtain

$$\varphi_{m_1} \cdots \varphi_{m_{k-1}} \varphi_{-\sum_{i=1}^{k-1} m_i} = \frac{1 + (-1)^k}{2} + 2 \sum_{n=1}^{k} (-1)^n \sum_{j_1=1}^{k} \cdots \sum_{j_n=j_{n-1}+1}^{k}$$

$$\begin{cases} \cos[(m_{j_1} + \ldots + m_{j_n})\omega_r t] & \text{for even } k \\ i\sin[(m_{j_1} + \ldots + m_{j_n})\omega_r t] & \text{for odd } k. \end{cases} \tag{19}$$

In Eq.(19), when k is an even number the product of k functions $\varphi_i (i=1 \ldots k)$ is also an even function of $N\omega_r t$; otherwise, it is odd. This means that even-order terms in the Taylor expansion add a symmetric correction to the intensities of the sidebands, whereas the odd terms create the differences in sideband intensities about the centerband. Because the odd terms are antisymmetric, they make no contribution to the centerband.

With substitution of Eqs.(15), (16), and (19) into Eq.(11), $\overline{f_k(t)}$ can be expressed by

$$\overline{f_k(t)} = \sum_{m=-2N}^{2N} \sum_{n=0}^{N} I_{k,m,n}\, \eta^{2n} \exp(-im\omega_r t)\ , \tag{20}$$

where $N = k/2$ and

$$I_{k,m,n} = \sum_{j=0}^{k} (-1)^j \sum_{l_1,\ldots,l_{k-3}} \sum_{m_1,\ldots,m_{k-1}\neq 0} \sum_{n_1,\ldots,n_{k-1}} B'(m_1,\ldots,m_{k-1}, -\sum_{i=1}^{k-1} m_i)$$

$$\times C(2,2,l_1;m_1,m_2)\, C(l_1,2,l_2;m_1+m_2,m_3) \ldots C(2,2,0,\sum_{i=1}^{k-1} m_i, -\sum_{i=1}^{k-1} m_i)$$

$$\times C(2,2,l_1;n_1,n_2)\, C(l_1,2,l_2;n_1+n_2,n_3) \ldots C(2,2,0,\sum_{i=1}^{k-1} n_i, -\sum_{i=1}^{k-1} n_i)$$

$$\times \varrho'_{2,n_1} \ldots \varrho'_{2,-\sum_{i=1}^{k-1} n_i} [\delta(m-\sum_{i=1}^{j} m_i) + (-1)^k\, \delta(m+\sum_{i=1}^{j} m_i)]\, \delta(2n-\sum_{i=1}^{k-1} \frac{|n_i|}{2}) \tag{21}$$

and where $B' = \delta^k B$. The ϱ'_{2m} are equal to $\varrho_{2,m}$, with $\delta = 1$ and $\eta = 1$ as given in Eq.(3).

From the definition of moments of a spectrum, the k-th moment can be written as

$$M_k = i^k \frac{d^k}{dt^k} g(t)|_{t=0}\ . \tag{22}$$

Inserting Eqs.(9) and (21) into Eq.(22) yields the relationship of the k-th moment with Fourier coefficients, $I_{k,m,n}$, given by

$$M_k = \sum_{m=-\infty}^{\infty} I_m\, \omega_r^m = \left(\sqrt{\frac{2}{3}}\omega_0\, \delta\right)^k \sum_{m=-2N}^{2N} \sum_{n=0}^{N} m^k\, I_{k,m,n}\, \eta^{2n}\ . \tag{23}$$

As the spinning speed increases, the sideband intensities, I_m, $(m \neq 0)$ decrease. The moments calculated by Eq.(23) from experimental spectra are therefore less accurate, and any anisotropic parameters subsequently extracted by the moment analysis method are inaccurate. However, the sideband intensities calculated by the Fourier coefficients, $I_{k,m,n}$, get closer to the actual values. In these circumstances, the approximate method proves to be an alternative to moment analysis. Another advantage is that the technique we propose is still valid for multi-site cases.

3. Results and Discussion

In the last Section, we have solved the powder average up to infinite order in the Taylor expansion of the FID signal. After substitution of Eqs.(11), (16), and (17) into (9), however, the FID signal can be represented as a Fourier series again (see Eq.(20)) and the sideband intensities can be obtained by evaluating the Fourier coefficients. As the order in the Taylor expansion increases, the number of summations over all Clebsch-Gordan coefficients also increases as $(k-3)$, where k is the k-th order in the expansion. Using a computer, it is easy to determine the coefficients of the first ten orders in the Taylor expansion, but calculation of higher-order coefficients becomes very time consuming. Fortunately, though, in practice the spinning speed typically is not much smaller than the CSA (especially for ^{13}C), and in these circumstances the approximation up to ninth order, as we will see, is already very good for the calculation of sideband intensities.

Here we only list the coefficients of the first four orders in the Taylor expansion and use them to draw some general properties of the sideband intensities under MAS. All other coefficients can be obtained from Eqs.(11), (14), (16), and (19), and the numerically calculated values of the Fourier coefficients, $I_{k,m,n}$, for values of index, k, from 2 to 9 are listed in Appendix in Tables 2 to 9. The expressions are

$$\overline{f_0(t)} = 1\,,$$

$$\overline{f_1(t)} = 0\,,$$

$$\overline{f_2(t)} = \frac{1}{5}(3+\eta^2)\left[-\frac{3}{4}+\frac{2}{3}\cos(\omega_r t)+\frac{1}{12}\cos(2\omega_r t)\right],$$

$$\overline{f_3(t)} = \frac{-3\mathrm{i}}{35}\sqrt{\frac{3}{2}}(-1+\eta^2)[2\sin(\omega_r t)-\sin(2\omega_r t)]\,. \qquad (24)$$

From Eq.(24) we note, first, that the zero-order term is always equal to one while the first-order term is zero. The first-order term therefore adds no correction to the first-order (± 1) sidebands regardless of the value of the asymmetry parameter, and consequently sideband intensities become more or less symmetric around the centerband once the spinning speed is larger than the linewidth of the static powder pattern. Such a distribution of sideband intensity which is no longer sensitive to η cannot be used to extract the anisotropic information.

Second, we observe that when $\eta = 1$ the value of $\overline{f_3(t)}$ is zero. This conclusion can be extended to all odd terms in accordance with the symmetry properties of odd and even orders in the Taylor expansion as discussed at

the end of the last Section. The static powder pattern is of course symmetric around the isotropic frequency once $\eta = 1$, and intuitively one would expect that the sidebands should also be symmetric around the centerband.

A third feature of Eq.(24) is that the sum of all coefficients of sidebands in $f_k(t)$ is always zero except for $k = 0$. The correction for each order just redistributes each sideband intensity over the whole set of sidebands, and the FID signal is always normalized. Finally, $f_k(t)$ is proportional to the k-th moments, arising from Eq.(23).

To test the accuracy of the approximate method we have to evaluate the sideband intensities exactly from Eq.(6). According to the result given by Herzfeld and Berger [7], the intensity of the N-th sideband is

$$I_N = \frac{1}{16\pi^4} \int_0^{\pi} \int_0^{2\pi} \sin(\beta) \mathrm{d}\beta \mathrm{d}\gamma \left| \int_0^{2\pi} \exp\{-\mathrm{i}[N\vartheta + \psi(\vartheta)]\} \mathrm{d}\vartheta \right|^2 , \quad (25)$$

where

$$\psi(\vartheta) = \sqrt{\frac{2}{3}} \frac{\omega_0}{-\mathrm{i}\omega_r} \sum_{m=-2}^{2} \frac{d^{(2)}_{m,0}(\vartheta_m)}{m} A_{2,m} \exp(-\mathrm{i}m\vartheta) . \quad (26)$$

Composite ten-point Gaussian (Gauss-Legendre) quadrature has been used to evaluate the three-dimensional integral in Eq.(26). Fig. 2 shows a comparison of sideband intensities computed through the first ten orders of the Taylor expansion (dashed line) with the exact solution (solid line) obtained by numerical simulation [7]. Since the ratio of the number of multiplications involved in the numerical integration of the exact solution given in Eq.(25) to that in the approximate method is at least on the order of 10^4, the computing time is reduced from about six hours on a Micro VAX II for the exact result to a few seconds for the approximate method. Both results are very close when the ratio of the anisotropy to the spinning speed, $\omega_0\delta/\omega_r$, is smaller than 3. For $\omega_0\delta/\omega_r > 3$, the sideband intensities calculated by the approximate method, however, tend to diverge. Fig. 3 shows the convergence under approximations of different order. We see that the sideband intensities converge at higher orders, and that the rate of convergence is much the same as for the sinusoidal functions. The total intensity obtained from the sum over all sideband intensities is always one, even though each sideband itself diverges. This is because the higher-order sideband intensities are given by redistributing the lower-order sideband intensities and keeping the whole intensity of the spectrum at unity. The divergence comes from an incorrect intensity partition for each sideband at large value of $\omega_0\delta/\omega_r$.

In practice, experimental sideband intensities have to be normalized for comparison with the theoretical values. Signal-to-noise therefore must be

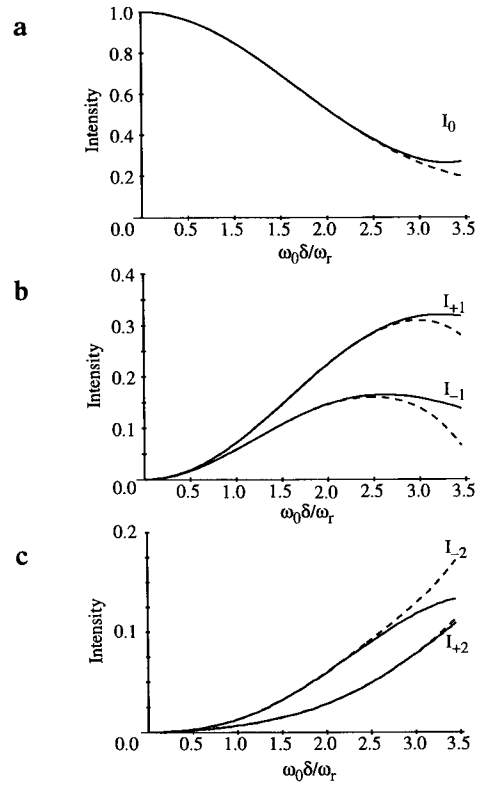

Fig. 2. Variation of sideband intensities with the ratio of chemical shift anisotropy ($\omega_0\delta$) to spinning speed (ω_r), computed for the case $\eta = 0.5$. Solid lines are calculated by numerically integrating Eq.(6) over all orientations, and dashed lines are obtained by our approximate method (up to the ninth order). **a** Centerband intensities. **b** First-order sidebands (±1). **c** Second-order sidebands (±2).

good enough to permit accurate measurement and summation of all sideband intensities. To overcome this requirement, Herzfeld and Berger proposed an alternative method in which the anisotropic information is extracted by measuring the ratios of the sideband intensities to the centerband intensity. Furthermore, as mentioned above, the differences of positive and negative sideband intensities around the centerband are relatively sensitive to the asymmetry factor (η), whereas the averages of these sideband intensities are sensitive only to the anisotropy (δ) (see Fig. 4). Although there is a maximum difference of the N-th order sideband intensities around the centerband, the change is minimized in axial and near-axial situations. This method therefore is only slightly better than the method used by Herzfeld and Berger. We use the ratios of the differences and averages to the centerband intensity to extract the anisotropic parameters by least squares fitting. In the fitting program (MASFIT), the initial values of the anisotropic par-

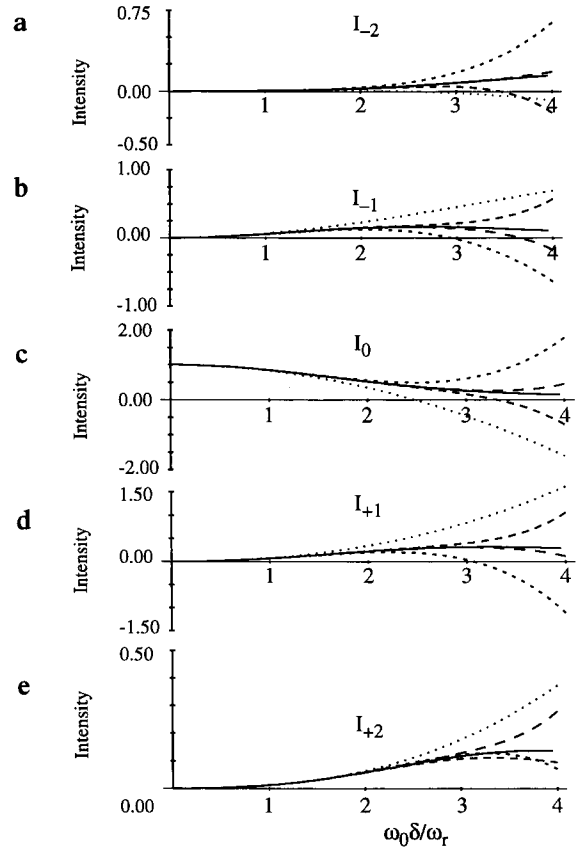

Fig. 3. Variation of sideband intensities with the ratio of chemical shift anisotropy ($\omega_0\delta$) to spinning speed (ω_r) under the approximate method, with first four (dotted lines), six (short dashed lines), eight (long dashed lines), and ten (solid lines) orders. $\eta = 0.5$. **a**, **e** Second-order sideband. **b**, **d** First-order sideband. **c** Centerband.

ameters are calculated by Eq.(24) and then, by use of the Davidon-Fletcher-Powell (DFP) algorithm [12], the anisotropic parameters can be extracted in a few seconds. Fig. 5 shows contours of the surface used in the fitting program. We can clearly see that there does exist a unique minimum, but that the surface is very smooth in the dimension of the asymmetry factor η. As a result, the determination of η is relatively less accurate than that of the anisotropy δ.

The overall quality of the fitting can be seen in Table 1. Fig. 6 shows that the experimental ^{31}P MAS spectrum of phosphorus pentoxide agrees well with the simulated spectrum by the approximate method. One severe problem appears when the asymmetry factor η is very small (that is, in the near-axial regime). Here the differences of the sideband intensities for different η

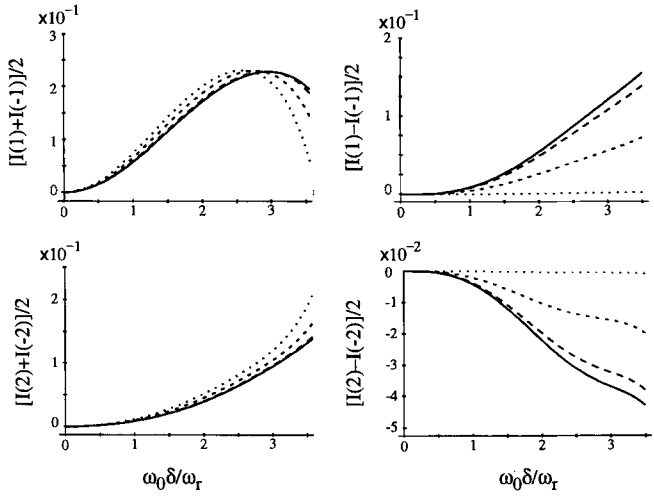

Fig. 4. Ratios of the differences and averages of positive- and negative-order sideband intensities to the centerband intensity as a function of $\omega_0\delta/\omega_r$ and the asymmetry factor (η). The four curves correspond to $\eta = 0$ (solid line), $\eta = 0.3$ (long dashed line), $\eta = 0.7$ (short dashed line), and $\eta = 1.0$ (dotted line).

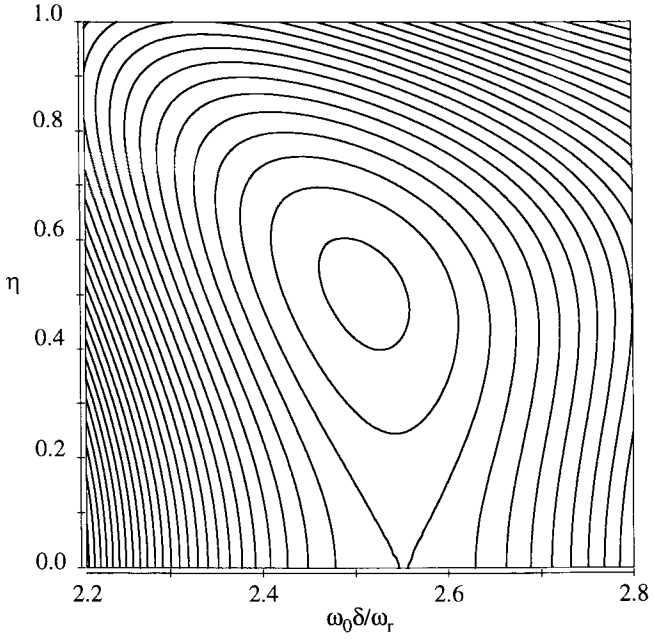

Fig. 5. Contour of the δ–η surface used in the least square fitting program, varying with $\omega_0\delta/\omega_r$ and η. The minimum corresponds to $\omega_0\delta/\omega_r = 2.5$, and $\eta = 0.5$.

Table 1. Results of sideband analysis.

	δ (ppm)	η
Lead Nitrate ($PbNO_3$) (^{207}Pb)		
Reported	35.4±3	0.0 ±0.16
Powder lineshape	35.9±5	0.0
Sideband	34.6±5	0.08±0.1
Benzoic Acid (^{13}C)		
Reported	71.0±4	0.6 ±0.12
Sideband	63.4±5	0.8 ±0.1
Phosphorus Pentoxide (^{31}P)		
Reported	218.0±20	0.0 ±0.18
Sideband	190.6±5	0.05±0.1
Powder lineshape	193.0±5	0.0

are so small (see also Fig. 5) that extraction of η becomes quite difficult. Such a problem exists both for moment analysis and powder lineshape simulation [13] methods.

Our approximate method also can be applied to calculate the centerband intensity after all sidebands are suppressed by a TOSS pulse sequence [8]. The FID signal of a spectrum with sidebands contains a series of rotational echoes. Moreover the rotational echo results from the periodicity of the

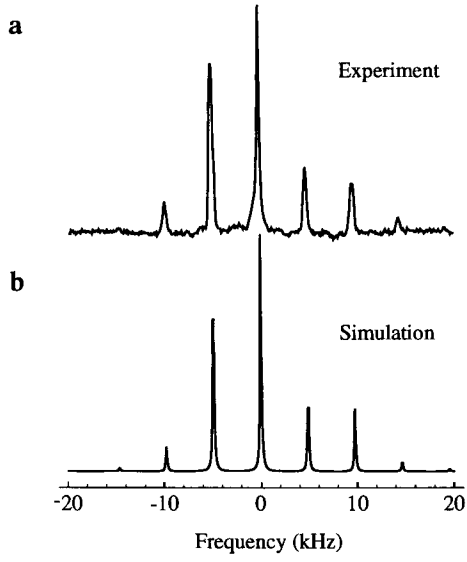

Fig. 6. Comparison of MAS spectrum simulated by the approximate method with the experimental results. **a** ^{31}P spectrum of solid phosphorus pentoxide, and **b** simulated spectrum with the principal values listed in Table 1.

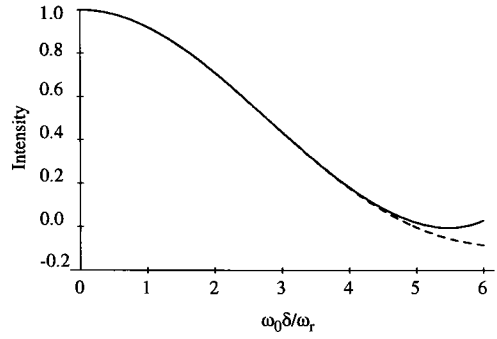

Fig. 7. Variation of centerband intensity with $\omega_0\delta/\omega_r$, at $\eta = 0.5$ after application of a TOSS pulse sequence.

phase, which runs from 0 to 2π over time. After TOSS, however, this period no longer exists [9], and then Eq.(8) must be replaced by

$$\varphi_m = \exp(-im\omega_r t), \tag{27}$$

leading to $\varphi_{m_1}\varphi_{m_2}\ldots\varphi_{m_k} = \exp(\Sigma_{i=1}^{k} m_i\omega_r t) = 1$ in Eq.(11), according to Eq.(15) after the power average. Thus $\overline{f_k(t)}$ is time independent, and $\overline{g(t)}$ gives the intensity of the centerband. From Eq.(18) and the properties of the Clebsch-Gordan coefficients, it can be found that $\overline{f_k(t)}$ are zero if k is an odd number. Fig. 7 shows the variation of the centerband intensity with the ratio of the anisotropy to the spinning speed, $\omega_0\delta/\omega_r$, at $\eta = 0.5$ in a TOSS experiment. It can be seen that, after TOSS, the centerband intensity converges much faster than does a normal MAS centerband.

4. Conclusions

We have shown that the FID signal under MAS can be expanded into a Taylor series which contains products of k irreducible spatial tensors ($k = 0...\infty$). The properties of irreducible tensors permit the integrals over all orientations to be solved analytically. The FID signal then becomes an expansion in a set of basis scalar operators, which are uniquely determined by the anisotropic parameters of the CSA tensors, and the coefficients in the expansion are given by a series of Clebsch-Gordan coefficients. After all the coefficients and the scalar operators are evaluated, the sideband intensities are functions of η^2, and the total pattern of sidebands can be understood as a sum of symmetric and antisymmetric parts about the centerband. The odd terms in the expansion determine the antisymmetric pattern, and make no contribution to the centerband intensity, while the even terms contribute to

the symmetric part. After manipulation of the Clebsch-Gordan coefficients, we obtain the approximate formula up to the ninth order in the Taylor expansion of the FID signal. Sideband intensities can be rapidly calculated using this formula even for spectra consisting of many different sites with overlapping sidebands. The results are in satisfactory agreement with the exact solution obtained by numerical simulation if the ratio of the anisotropy to the spinning speed, $\omega_0\delta/\omega_r$, is smaller than 3. The relationship of the Fourier coefficients, $I_{k,m,n}$ is given in Eq.(23), and shows that the moment analysis method is valid in the slow spinning regime whereas our approximate method is an alternative choice if the spinning speed is not very slow. The anisotropic parameters can be extracted very efficiently using this method combining with least-squares fitting methods. We have also applied the technique to calculate the centerband intensity after eliminating the sidebands using a TOSS pulse sequence in MAS, and shown that the centerband intensity after TOSS converges to the exact value much faster than for MAS. The technique may also be applied to sideband intensity calculation in double rotation (DOR) [14–17], and dynamical angle spinning (DAS) [18, 19] NMR.

Appendix

The numerically calculated values of the Fourier coefficients, $I_{k,m,n}$, of MAS sideband intensities used in Eq.(21) for values of index, k, from 2 to 9 are listed in Tales 2 to 9. In the calculation, double precision numbers were used.

Table 2. Numerically calculated values of the Fourier coefficients $I_{2,m,n}$.

n	0	1
−2	0.025000	0.008333
−1	0.200000	0.066667
0	−0.450000	−0.150000
1	0.200000	0.066667
2	0.025000	0.008333

Table 3. Numerically calculated values of the Fourier coefficients $I_{3,m,n}$.

n	0	1
−2	0.052489	−0.052489
−1	−0.104978	0.104978
0	0.000000	0.000000
1	0.104978	−0.104978
2	−0.052489	0.052489

Table 4. Numerically calculated values of the Fourier coefficients $I_{4,m,n}$.

n	0	1	2
−4	0.001339	0.000893	0.000149
−3	0.021429	0.014286	0.002381
−2	0.037500	0.025000	0.004167
−1	−0.364286	−0.242857	−0.040476
0	0.608036	0.405357	0.067560
1	−0.364286	−0.242857	−0.040476
2	0.037500	0.025000	0.004167
3	0.021429	0.014286	0.002381
4	0.001339	0.000893	0.000149

Table 5. Numerically calculated values of the Fourier coefficients $I_{5,m,n}$.

n	0	1	2
−4	0.005965	−0.003976	−0.001988
−3	0.035788	−0.023859	−0.011929
−2	−0.202798	0.135199	0.067600
−1	0.274374	−0.182917	−0.091459
0	0.000000	0.000000	0.000000
1	−0.274374	0.182917	0.091459
2	0.202798	−0.135199	−0.067600
3	−0.035788	0.023859	0.011929
4	−0.005965	0.003976	0.001988

Table 6. Numerically calculated values of the Fourier coefficients $I_{6,m,n}$.

n	0	1	2	3
−6	0.000088	0.000111	0.000024	0.000004
−5	0.002107	0.002669	0.000578	0.000085
−4	0.018860	−0.008254	0.012312	0.000364
−3	−0.055773	0.057927	−0.043857	−0.000662
−2	−0.157148	−0.327617	−0.014499	−0.007925
−1	0.772950	0.850491	0.240416	0.029585
0	−1.162166	−1.150597	−0.389944	−0.042902
1	0.772950	0.850491	0.240416	0.029585
2	−0.157148	−0.327617	−0.014499	−0.007925
3	−0.055773	0.057927	−0.043857	−0.000662
4	0.018860	−0.008254	0.012312	0.000364
5	0.002107	0.002669	0.000578	0.000085
6	0.000088	0.000111	0.000024	0.000004

Table 7. Numerically calculated values of the Fourier coefficients $I_{7,m,n}$.

n	0	1	2	3
−6	0.000602	−0.000201	−0.000335	−0.000067
−5	0.008431	−0.002810	−0.004684	−0.000937
−4	−0.002409	0.000803	0.001338	0.000268
−3	−0.196319	0.065444	0.109066	0.021812
−2	0.619605	−0.206561	−0.344274	−0.068848
−1	−0.686391	0.228852	0.381443	0.076267
0	0.000000	0.000000	0.000000	0.000000
1	0.686391	−0.228852	−0.381443	−0.076267
2	−0.619605	0.206561	0.344274	0.068848
3	0.196319	−0.065444	−0.109066	−0.021812
4	0.002409	−0.000803	−0.001338	−0.000268
5	−0.008431	0.002810	0.004684	0.000937
6	−0.000602	0.000201	0.000335	0.000067

Table 8. Numerically calculated values of the Fourier coefficients $I_{8,m,n}$.

n	0	1	2	3	4
−8	0.000006	0.000013	0.000005	0.000001	0.000000
−7	0.000202	0.000424	0.000152	0.000020	0.000003
−6	0.003362	−0.000260	0.001715	0.000791	0.000022
−5	0.007780	−0.012918	0.002599	0.002590	0.000000
−4	−0.108238	0.109288	−0.043981	−0.031687	−0.000293
−3	0.153059	−0.526660	0.020917	0.067815	−0.001116
−2	0.461523	1.558837	0.412428	0.010160	0.009588
−1	−1.819799	−2.937437	−1.269512	−0.237990	−0.024564
0	2.601998	3.618606	1.750050	0.376696	0.032788
1	−1.819799	−2.937437	−1.269512	−0.237990	−0.024564
2	0.461523	1.558837	0.412428	0.010160	0.009588
3	0.153059	−0.526660	0.020917	0.067815	−0.001116
4	−0.108238	0.109288	−0.043981	−0.031687	−0.000293
5	0.007780	−0.012918	0.002599	0.002590	0.000000
6	0.003362	−0.000260	0.001715	0.000791	0.000022
7	0.000202	0.000424	0.000152	0.000020	0.000003
8	0.000006	0.000013	0.000005	0.000001	0.000000

Table 9. Numerically calculated values of the Fourier coefficients $I_{9,m,n}$.

n	0	1	2	3	4
−8	0.000024	0.000005	−0.000022	−0.000006	−0.000001
−7	0.000446	−0.000013	−0.000281	−0.000135	−0.000016
−6	0.002362	−0.001004	−0.000347	−0.000935	−0.000075
−5	−0.010645	0.008727	−0.003569	0.005201	0.000287
−4	−0.061344	−0.033566	0.081922	0.010302	0.002686
−3	0.397052	0.074909	−0.356256	−0.100074	−0.015630
−2	−0.871551	−0.102989	0.706910	0.234079	0.033551
−1	0.833058	0.077968	−0.650666	−0.228543	−0.031817
0	0.000000	0.000000	0.000000	0.000000	0.000000
1	−0.833058	−0.077968	0.650666	0.228543	0.031817
2	0.871551	0.102989	−0.706910	−0.234079	−0.033551
3	−0.397052	−0.074909	0.356256	0.100074	0.015630
4	0.061344	0.033566	−0.081922	−0.010302	−0.002686
5	0.010645	−0.008727	0.003569	−0.005201	−0.000287
6	−0.002362	0.001004	0.000347	0.000935	0.000075
7	−0.000446	0.000013	0.000281	0.000135	0.000016
8	−0.000024	−0.000005	0.000022	0.000006	0.000001

References

[1] Andrew E.R., Bradbury A., Eades R.G.: Nature **182**, 1659 (1958)
[2] Andrew E.R.: Arch. Sci. (Geneva) **12**, 103 (1959)
[3] Lowe I.J.: Phys. Rev. Lett. **2**, 285 (1959)
[4] Schaefer J., Stejskal E.O.: J. Am. Chem. Soc. **98**, 1031 (1976)
[5] Bloch F.: Phys. Rev. **94**, 496 (1954)
[6] Maricq M.M., Waugh J.S.: J. Chem. Phys. **70**, 3300 (1979)
[7] Herzfeld J., Berger A.E.: J. Chem. Phys. **73**, 6012 (1980)
[8] Dixon W.T.: J. Chem. Phys. **77**, 1800 (1982)
[9] Raleigh D.P., Olejniczak E.T., Vega S., Griffin R.G.: J. Magn. Reson. **72**, 238 (1986)
[10] Mehring M.: Principles of High Resolution NMR in Solids, 2nd ed. Berlin: Springer-Verlag 1983.
[11] Rose M.E.: Elementary Theory of Angular Momentum. New York: John Wiley & Sons 1957.
[12] Press W.H., Flannery B.P., Teukolsky S.A., Vetterling W.T.: Numerical Recipes. New York: Cambridge University Press 1988.
[13] Clayden N.J., Dobson C.M., Lian L.Y., Smith D.J.: J. Magn. Reson. **69**, 476 (1986)
[14] Samoson A., Lippmaa E., Pines A.: Mol. Phys. **65**, 1013 (1988)
[15] Chmelka B.F., Mueller K.T., Pines A., Stebbins J., Wu Y., Zwanziger J.W.: Nature (London) **339**, 42 (1989)
[16] Wu Y., Sun. B.-Q., Pines A., Samoson A., Lippmaa E.: J. Magn. Reson. **89**, 296 (1990)
[17] Sun B.-Q., Baltisberger J., Wu Y., Samoson A, Pines A.: Solid State-Nuclear Magnetic Resonance **1**(5), 267 (1992)
[18] Llor A., Virlet J.: Chem. Phys. Lett. **152**, 248 (1988)
[19] Mueller K.T., Sun B.-Q., Chingas G.C., Zwanziger J.W., Terao T., Pines A.: J. Magn. Reson. **86**, 470 (1990)

Author's address: Prof. Dr. A. Pines, Materials and Chemical Sciences Division, Lawrence Berkeley Laboratory, 1 Cyclotron Road, Berkeley, CA 94720; and Chemistry Department, University of California, Berkeley, CA 94720, USA